# Diffusion Limited Escape of Hydrogen from Mars

Roger V. Yelle[a]

[a]*Department of Planetary Sciences, University of Arizona, Tucson AZ 85721*

**Abstract**

Hydrogen escapes from Mars primarily by the Jeans mechanism but the rate is variable and the controlling factors complicated. One of the complications is that the temperature at the Martian exobase varies from ∼100 K in the early morning hours to ∼300 K in the afternoon. At the cold temperatures on the nightside of Mars, H escape rate is limited by the Jeans escape, but on the warm dayside H escape is limited by the diffusion rate through the thermosphere. Nevertheless, the hot and cold regions are coupled by efficient ballistic transport through the exosphere. Because of this, H diffuses upward at the diffusion-limited rate even on the nightside and, once H reaches the exosphere, it is transported rapidly by ballistic flow to the warm dayside, where it escapes. As a result, escape is not at all limited by the cold regions of the exobase. The globally integrated escape flux is be equal to the globally integrated diffusive limit. Because of this it is important to precisely calculate the diffusion-limited flux and we present a new formulation that is significantly more accurate than the classical formula.

*Keywords:* , Hydrogen, Mars, Escape

## 1. Introduction

If we want to understand the evolution of the surface and atmosphere on Mars we have to understand H escape. The only important reservoir of H on present day Mars is $H_2O$ and H escape is a primary $H_2O$ destruction mechanism on evolutionary time scales (Jakosky, 2021). Recent observations from the MEX, MAVEN, and TGO missions have revolutionized our understanding of H escape, showing that the rates are highly variable and correlated with dust loading of the atmosphere (Chaffin et al., 2014; Clarke et al., 2014; Bhattacharyya et al., 2015; Chaffin et al., 2017; Halekas, 2017; Heavens et al., 2018; Fedorova et al., 2018, 2020; Aoki et al., 2019; Stone et al., 2020; Chaffin et al., 2021). Because these missions make local measurements of density and temperature, it is challenging to develop an understanding of H escape on a global scale (Chaffin et al., 2014, 2017; Bhattacharyya et al., 2020; Stone et al., 2020). Nevertheless, H escape from Mars is intrinsically a global phenomenon and an important part of this is horizontal coupling associated with efficient ballistic transport through the exosphere.

Most previous investigations of H escape on Mars have focussed on the roles played by Jeans (thermal) escape and diffusion through the thermosphere. It is well established the hydrogen escape from Mars is primarily thermal with, perhaps, a small contribution from non-thermal processes (Bhattacharyya et al., 2023; Cangi et al., 2023). It is less clear that the thermal escape rate is limited by the diffusion rate through the thermosphere. There are different assumptions and conclusions about this in the literature (Krasnopolsky, 1993; Fox, 1993; Zahnle et al., 2008; Chaufray et al., 2015). The exospheric temperature on Mars varies from roughly 100 K to 300 K.

At the lowest temperatures, weak H escape does not affect the H density profile and escape rates are limited by the temperature at the exobase, but at the higher temperatures, escape does strongly affect the H density profile and escape is limited by the diffusion rate. It is unclear what this means for the global escape rate on a planet with wide temperature variations and this topic has received little attention to date. Nevertheless, the way that a diurnally varying thermal escape and diffusion interact is critical to an understanding of H escape on Mars and, as we discuss below, the nature of the interaction is unique to Mars, at least in this solar system.

The first step in this investigation is a review of the classical theory of diffusion-limited escape. An extention of this theory is described, making it more complicated but significantly more accurate. Following that are presented some considerations of how flow though the exosphere affects diffusion through the thermosphere. The two processes are strongly coupled and have a large affect on the distribution of H across the Martian exobase. One consequence of this coupling is that H diffuses upward at the limiting rate at all locations around the planet. The globally integrated escape rate should be equal to the globally integrated limiting flux even though large areas of the planet may have temperatures too low to support rapid escape.

## 2. Solutions to the Diffusion Equation

The vertical diffusion equation is usually written as

$$\Phi_i = -D_i \left[ \frac{dN_i}{dr} + N_i \left( \frac{1}{H_i} + \frac{1+\alpha}{T} \frac{dT}{dr} \right) \right] - K \left[ \frac{dN_i}{dr} + N_i \left( \frac{1}{H_a} + \frac{1}{T} \frac{dT}{dr} \right) \right] \quad (1)$$

where $\Phi_i$ the flux of the $i$th constitutent, $N_i$ is its density, $H_i$ its scale height, and $D_i$ its molecular diffusion coefficient. The quantity $T$ is the atmospheric temperature, $H_a$ the atmospheric scale height, and $K$ the eddy diffusion coefficient. This equation appears in numerous landmark papers and textbooks (Colegrove et al., 1965; Hunten, 1973; Banks and Kockarts, 1973; Chamberlain and Hunten, 1986). A more convenient form for this equation is obtained by using mole fraction, $X_i = N_i/N_a$, in place of density and log pressure in place of altitude. Equation 1 becomes

$$\frac{dX_i}{d\zeta} + \frac{D_i(\tilde{m}_i/m_a - 1)}{D_i + K} X_i + \frac{r_\circ^2 \Phi_i^\circ kT}{GMm_a N_a (D_i + K)} = 0\,, \tag{2}$$

where $r_\circ$ is a reference radial distance, $m_i$ is the mass of a hydrogen atom, $m_a$ is the mean molecular mass of the atmosphere, $M$ the mass of Mars, and and $\Phi_i^\circ$ is the flux at $r_\circ$. If there is no significant chemical production or loss then $r^2\Phi_i = r_\circ^2\Phi_i^\circ =$ constant. Good choices for $r_\circ$ include the surface radius or the homopause radius, but any value is legitimate and the choice is at the discretion of the investigator. Equation 2 uses the log of pressure as the vertical variable, defined through

$$\zeta \equiv -\ln(p/p_\circ)\,. \tag{3}$$

where $p_\circ$ is the pressure at $r_\circ$. Also, the mass of the diffusing constituent appearing in equation 2 is an effective mass defined through

$$\tilde{m}_i = m_i + \alpha \frac{m_a}{T}\frac{dT}{d\zeta} \tag{4}$$

where $\alpha$ is the thermal diffusion coefficient. A value of $\alpha = -0.25$ is used here (Banks and Kockarts, 1973). The limiting flux follows directly from equation 2. For H to escape from the top of the atmosphere there must be

some H atoms at the highest altitudes where the escape processes operate. For there to be significant density at the exobase, the derivative of the mole fraction with altitude should be greater than zero (Hunten, 1973). The limit is obtained for $dX_i/d\zeta = 0$. Substituting this into equation 2 gives

$$\Phi_i = X_i \frac{b}{H_a}\left(1 - \tilde{m}_i/m_a\right), \tag{5}$$

where

$$b(T) = DN_a \tag{6}$$

is the binary diffusion parameter, a function only of temperature, and

$$H_a = \frac{kT_\circ r_\circ^2}{GMm_a} \tag{7}$$

is the atmospheric scale height at $r_\circ$. Equation 5 is the classical expression for Hunten's limiting flux (Hunten, 1973) with only a slight correction for thermal diffusion, which was ignored in the original derivation. In practical terms, inclusion of thermal diffusion has little effect on the calculations presented below and is included only for completeness.

The diffusion equation is simple enough that a more sophisticated analysis is possible. The general solution to equation 2 can be written as

$$X_i(\zeta) = \tilde{X}_i(\zeta)\left(1 - g(\zeta)\Phi_i^\circ\right) \tag{8}$$

where $\tilde{X}_i$ is the diffusive equilibrium (zero flux) solution given by

$$\tilde{X}_i(\zeta) = \tilde{X}_i(0)\exp\left\{\left(\int_0^\zeta \left(1 - \frac{\tilde{m}_i}{m_a}\right)\frac{D_i(\zeta')}{D_i(\zeta') + K(\zeta')}\,d\zeta'\right)\right\} \tag{9}$$

and $g(\zeta)$ is an auxiliary function defined by

$$g(\zeta) \equiv \int_0^\zeta \frac{kT(\zeta')r_\circ^2\,d\zeta'}{\tilde{X}_i(\zeta')\big(D_i(\zeta') + K(\zeta')\big)N_a(\zeta')GMm_a}\,. \tag{10}$$

We can now apply an argument similar to that used before except that instead of requiring $dX_i/d\zeta = 0$ we simply require that $X_i(\zeta_x) = 0$ at the exobase, $\zeta_x$. This leads to

$$\Phi_i^\circ = \frac{1}{g(\zeta_x)} \equiv \Phi_\ell \,. \tag{11}$$

Equation 11 defines a new form for the limiting flux, $\Phi_\ell$, that is more complicated than the classical formula (equation 5) but is based on rigorous solution of the diffusion equation. One critical difference is that this new form for the limiting flux depends on the eddy diffusion coefficient and the temperature profile whereas the classical expression did not.

The limiting flux defined in equation 11 plays a central role in solutions of the actual escape flux and in calculations of the mole fraction of the escaping species. The escape flux is related to the mole fraction at the exobase through the Jeans boundary condition:

$$\Phi_i^\circ = \left(\frac{r_x}{r_\circ}\right)^2 w_J(\zeta_x) X_i(\zeta_x) N_a(\zeta_x) \,, \tag{12}$$

where $r_x$ is the radius of the exobase. Evaluating equation 8 at the exobase relates the mole fraction at the exobase to the diffusive equilibrium solution and the escape flux:

$$X_i(\zeta_x) = \tilde{X}_i(\zeta_x)\left(1 - \frac{\Phi_i^\circ}{\Phi_\ell}\right) . \tag{13}$$

Equation 13 clearly shows that if $\Phi_i^\circ << \Phi_l$ the mole fraction at the exobase is approximately equal to the diffusive equilibrium value: diffusion and escape have had little effect on the distribution of the escaping constituent. Combining equations 12 and 13 gives

$$\Phi_i^\circ = \frac{\tilde{\Phi}_i \Phi_\ell}{\tilde{\Phi}_i + \Phi_\ell} \,, \tag{14}$$

where

$$\tilde{\Phi}_i = \left(\frac{r_x}{r_\circ}\right)^2 w_J(\zeta_x)\tilde{X}(\zeta_x)N_a(\zeta_x)\,, \tag{15}$$

is the escape flux calculated using the diffusive equilibrium solution. If $\tilde{\Phi}_i << \Phi_l$ then $\Phi_i^\circ = \tilde{\Phi}_i$ and the escape flux has little effect on the distribution of the escaping constituent. On the other hand, if $\tilde{\Phi}_i >> \Phi_l$ then $\Phi_i^\circ = \Phi_\ell$. It is worth emphasizing that the limiting flux defined in equation 11 is a real limit to the escape flux, not an approximation. This is an improvement over the original definition to the limiting flux, which is only an approximation to the escape flux even in the diffusion limit. Results illustrating this are presented below.

Substituting equation 14 into equation 13 gives

$$\frac{X_i(\zeta_x)}{\tilde{X}_i(\zeta_x)} = \frac{\Phi_\ell}{\tilde{\Phi}_i + \Phi_\ell}\,. \tag{16}$$

Clearly if $\tilde{\Phi}_i << \Phi_\ell$ then $X_i(\zeta_x) \sim \tilde{X}_i(\zeta_x)$ and the actual solution is approximately equal to the diffusive equilibrium solution: diffusion and escape have had little effect on the distribution of the escaping constituent. On the other hand if $\tilde{\Phi}_i >> \Phi_\ell$ then $X_i(\zeta_x) << \tilde{X}_i(\zeta_x)$; the mole fraction at the exobase is far below the diffusive equilibrium value. This, of course, is related to the throttling of the escape rate by diffusion through the thermosphere, the 'choking off of the flow' recognized by Hunten (1973). The decreased value of $X_i(\zeta_x)$ leads to a decreased escape flux through equation 12.

A better understanding of the relationship between the approach described here and that in Hunten (1973) can be obtained by assuming a constant temperature, that $D >> K$, and that $\alpha = 0$. The diffusive equilibrium

solution under these assumptions is

$$\tilde{X}_i(\zeta) = \tilde{X}_i(0) e^{(1-m_i/m_a)\zeta}\,, \tag{17}$$

and the limiting flux, defined by equation 11, becomes

$$\Phi_\ell(\zeta_x) = \tilde{X}_i(0) \frac{b(1-m_i/m_a)}{H_a} \left(1 - e^{(m_i/m_a - 1)\zeta_x}\right), \tag{18}$$

which is equal to Hunten's limiting flux if $\zeta_x = \infty$. The final factor on the RHS of equation 14 is, in fact, rather close to 1; thus, the difference between the limiting flux defined here and the classical result is primarily due to the effects of the temperature gradient and eddy mixing near the homopause.

The limiting flux has several uses. Because it is easy to calculate it can, in some situations, be used as an approximation to the actual escape flux if the complexity of a full solution of the diffusion equation is not justified. Examples include estimates of escape fluxes from poorly understood systems such as exoplanets or early solar system atmospheres or interpretation of escape measurements from largely observational studies. The limiting flux in these situations allows an investigator to estimate the escape flux with a simple calculation. The limiting flux also gives insight into the physical processes in the atmosphere. If the escape flux is close to the limiting flux then diffusion through the upper atmosphere is the controlling process for escape. This can be helpful because it might allow one to ignore the details of chemistry or other complications in the atmosphere. The approach to be followed depends on the escape regime, which can be determined by calculation of $\Phi_l$ from equation 11 and $\tilde{\Phi}_i$ from equation 12. These two quantities, along with the other relations presented above determine if the diffusion plays a role in limiting the escape flux.

The formulation just presented is appropriate for a minor constituent diffusing through a stationary background atmosphere. However, here $X_i$ is viewed as the total mixing ratio of atomic hydrogen, summed over all H-bearing molecular constituents: H, $H_2$, and $H_2O$. The assumption, inherent in the limiting flux analysis, is that chemistry may cause interchange among the molecular reservoirs of H, but, of course, not the total H abundance and, as long as the diffusion properties of the various constituents are not too different, the formulae above apply. What is really required is to know the identity of the H-bearing molecules near the homopause so that the proper value of binary diffusion parameters, $b$, is chosen and the number of H atoms accounted for correctly. It is also necessary that H be converted to atomic form by chemistry in the upper atmosphere. This approach has been discussed extensively in the early literature on the limiting flux (Hunten, 1973).

The implications of the new formula for the limiting flux can be illustrated by comparison with 1D models for H diffusion and escape from the Martian atmosphere. The calculations extend from the mesopause to the exobase. The bottom boundary of the model is set at 80 km where we assume a pressure of $p_\circ = 0.1\,\mathrm{Pa}$. The top of the model is at a pressure of $10^{-6}\,\mathrm{Pa}$ which is roughly the exobase. The models are one dimensional, include diffusion, but neglect chemistry. The models use an eddy diffusion coefficient of $K = 3 \times 10^6\,\mathrm{cm^2\,s^{-1}}$ (**?**) and temperature profile given by

$$T(\zeta) = T_\circ + \left(T_\infty - T_\circ\right)\left(1 - e^{-0.75\zeta}\right). \tag{19}$$

This analytic formula is equivalent to a Bates profile and gives a good representation of the temperature profiles for the Mars thermosphere derived in Stone et al. (2018). We set $T_\circ = 100\,\mathrm{K}$ and examine solutions for a range

of exospheric temperatures, $T_\infty$. The H mole fraction at the bottom on the model is fixed at $10\times10^{-6}$, which leads to an escape flux of $2.4\times10^8\,\mathrm{cm^{-2}\,s^{-1}}$ in agreement with **?**). We set the diffusion velocity at the exobase equal to the Jeans escape velocity

$$w_J(T_\infty) = \frac{1}{2\sqrt{\pi}}\sqrt{\frac{2kT_\infty}{m_i}}(1+\lambda)e^{-\lambda}\,, \tag{20}$$

where

$$\lambda = \frac{GMm_i}{kT_\infty r_x}\,. \tag{21}$$

These models are simple, focussing only on the diffusion equation and Jeans escape. H escape from Mars is more complicated than this but the goal here is to investigate some properties of the diffusion equation and these simple models enable that.

The escape flux calculated from these models is shown in Fig. 1. Also shown in the figure are the limiting flux defined above and the classical limiting flux (equation 5). At low temperatures the escape flux increases rapidly with temperature. These fluxes are smaller than the limiting flux, the density at the exobase is roughly constant, and the temperature variation in the escape flux reflects the dependence of the Jeans velocity on temperature. At these low temperatures the escape of H is, essentially, limited by kinetics. For temperatures above $\sim$150 K the increase of flux with temperature stops. The atmosphere is in the limiting flux situation and the escape flux is well approximated by the new limiting flux. The escape flux in this region is roughly a factor of 2 larger than the classical limiting flux (near $T_\infty = 300\,\mathrm{K}$) but precisely equal to the limiting flux proposed here.

The calculations shown here are for an eddy coefficient that is constant

with altitude and equal to $3\times10^6\,\mathrm{cm^2\,s^{-1}}$ . Smaller values of the eddy coefficient would produce better agreement between the limiting flux proposed here and the classical limiting flux; larger values would produce worse agreement. In all case though, the actual solution is quite similar to that shown in Fig. 1 and the limiting flux proposed here is very nearly equal to the calculated escape flux for temperatures above 150 K.

Fig. 2 shows the H densities at the exobase calculated with the 1D model. At low temperature, in the limit of $\tilde{\Phi}_i << \Phi_\ell$, the H density at the exobase is equal to the diffusive equilibrium solution. As the temperature increase, the density drops rapidly to offset the increase in the Jeans velocity under the constraints of a roughly constant flux. At high temperatures, if $\tilde{\Phi}_i >> \Phi_\ell$, the H density at the exobase is given by

$$N_H(\zeta_x) = \frac{\Phi_\ell}{w_J(T_\infty)} \tag{22}$$

and the density varies inversely with the temperature dependence of the Jeans velocity. The strong dependence of exobase density on temperature has important implications for Mars that we discuss in the next section.

Fig. 2 shows the profile of H mole fraction versus log pressure. At low altitude (high pressure) the H mole fraction is constant because of the effects eddy diffusion. Although it depends slightly on the temperature profile the homopause ($K = D$) for these models is located near $\zeta = 3$. For the models with low $T_\infty$, $X(\zeta)$ begins to increase at altitudes just above this level, in accord with diffusive equilibrium. For larger values of $T_\infty$, $X(\zeta)$ rises more slowly because of the effects of the upward flux until for the highest values of $T_\infty$ $X(\zeta)$, does not increase substantially until the top of the atmosphere, above $\zeta \sim 8 - 9$.

## 3. Models Including Ballistic Fluxes

Figure 3a shows the exospheric temperature derived by Stone et al. (2018) from MAVEN/NGIMS measurements and are also in rough agreement with the temperatures calculated by Chaufray et al. (2015) for perihelion season. The exospheric temperature exhibits large diurnal variations with temperatures in the early morning hours approaching 100 K and temperatures in the afternoon approaching 300 K. The range of exospheric temperatures spans the regions where, according to Fig. 1, escape is kinetically limited to the region where escape is diffusion limited. In our solar system, this situation is unique to Mars. On Earth, exospheric temperatures are large enough that H escape is diffusion limited at all local times and latitudes (Park et al., 2022). The situation is similar for $H_2$ escape on Titan (Cui et al., 2008). On Venus, the exospheric temperature is so low that H escape is never diffusion limited (Gérard et al., 2017). Of course, there may be terrestrial exoplanets that are similar to Mars, especially tidally-locked exoplanets, but these have yet to be characterized.

Figure 3a also shows the H density at the exobase calculated with a 1D diffusion model using the Jeans velocity as the upper boundary condition (magenta curve). Because the exospheric temperatures spans the range from kinetic limited to diffusion limited, the calculated H density variation with local time is large, roughly 3 orders of magnitude. The strong variation is consistent with the rapid drop in exobase density with temperature shown in Fig. 1. This introduces a problem: the atmosphere of Mars cannot maintain the large density variations just derived. The reason is that H atoms are quickly transported horizontally by ballistic flight through the exosphere.

H is a minor constituent in the upper atmosphere of Mars and the exobase on Mars is determined by the $CO_2$ density profile. Moreover, the H scale height is 44 times larger than the $CO_2$ scale height; thus, though H is a minor constituent in the thermosphere, it becomes the dominant constituent above the exobase. The dominant circulation pattern in the thermosphere is day-to-night flow driven by the warmer dayside temperatures (Bougher et al., 2015; Roeten et al., 2019, and references therein). The frequent collisions in the thermosphere force H and other minor constituents to flow along with the $CO_2$. This produces the night-side enhancements in light minor constituents seen in numerous species (Elrod et al., 2017; Gupta et al., 2021; Stone et al., 2022). However, because H dominates the exosphere it is free to flow in response to density variations and, because collisions are rare, the flow is manifest as ballistic trajectories from high density regions to low density regions. Ballistic transport is highly efficient for H because of its large scale height, roughly 750 km for a temperature of 300 K. The average ballistic hop distance is roughly equal to the scale height implying that one ballistic hop can cover a significant horizontal distance on the exobase (Hodges and Johnson, 1968). The average hop lasts only 5 or 6 minutes implying that diurnal density variations at the exobase can be smoothed out on a time scale shorter than one day. Thus, ballistic transport will act to smooth out large density variations driven by the diurnal variation in escape flux.

Winds in the thermosphere flow to minimize pressure gradients but the nature of flow in the exosphere is different. The characteristics and implications of ballistic transport have been studied by Hodges and Johnson (1968) who showed that, in the limit of highly efficient ballistic transport,

the exobase density varies such that $NT^{2.5}$ = constant, rather than constant pressure. More recently, Chaufray et al. (2018) used an exospheric transport model coupled to a general circulation model (GCM) to show ballistic transport is highly efficient on Mars. These authors found that the value of $NT^{2.5}$ varied by a factor of $\sim 2$ over the exobase. If we assume that the Hodges and Johnson relation applies, then the implied density variation at the exobase is far smaller than that calculated earlier ignoring ballistic transport. The Hodges and Johnson relation implies a factor of 13 variation in the exobase H density, assuming the Stone et al. (2018) diurnal variation in temperature. Even if this is off by a factor of 2, the variation is far smaller than the factor of 1000 variation calculated earlier in this paper using the Jeans escape velocity as the upper boundary condition in a 1D model. The mild variation in exobase density implied by the Hodges and Johnson formula (or anything close to it) requires the presence of ballistic fluxes for exobase H densities to be consistent with solutions of the diffusion equation.

Model calculations assuming $NT^{2.5}$ = constant illustrate the effects of ballistic transport on the H escape rate. The models use the exospheric temperature variation from Stone et al. (2018), which is appropriate for the equatorial regions. The value of the H flux at the exobase as a function of local time is adjusted to produce an H density at the exobase that varies as $T^{-2.5}$. The boundary flux is equal to the sum of the local ballistic flux and escape flux, calculated from the Jeans velocity. It is also required that, integrated over local time, the upward and downward ballistic fluxes balance. This leads to a unique solution for the H distribution. Results are shown in Figs. 3a and 3b. The calculated H density at the exobase is shown in Fig. 3a.

There is a minimum in density in the afternoon when the temperature is highest, but the minimum is much smaller than calculated without the presence of ballistic fluxes. More surprisingly, the H density is everywhere much smaller than the diffusive equilibrium solution, implying there is upward flux at all local times. In fact, the density is orders of magnitude less than the diffusive equilibrium density implying that, according to equation 12, the diffusive flux must be nearly equal to the limiting flux. This is shown in Fig. 3b where the flux required to produce the $T^{-2.5}$ behavior is essentially identical to the limiting flux defined by equation 10. The model shows that, in order to produce the relatively mild $T^{-2.5}$ density variation at the exobase, flow must be diffusion-limited in cold, as well as hot, regions of the planet. The altitude variation of H mole is shown in Fig. 4.

The existence of an upward flux at all local times does not violate flux conservation. The reason is revealed in Fig. 3b. Although the net flux is positive at all local times the ballistic flux is strongly negative in the afternoon where the temperatures are high. The net flux in this local time range is still positive because the escape flux is positive and larger in absolute magnitude than the ballistic flux. In fact, the ballistic flow allows the escape flux to exceed the diffusive limit on the warm dayside. Most of the H atoms escaping from the dayside are supplied by ballistic flow through the exosphere, not diffusion through the thermosphere.

The physical explanation for this behavior is illustrated in Fig. 5. The strong escape in the afternoon results in a depletion of H. Atoms on ballistic trajectories from colder atmospheric regions flow to the warm dayside where they soon escape. In order to supply these atoms to the exobase, the diffusive

flow through the thermosphere must be at the maximum rate. H atoms flow upward at the maximum rate everywhere then are transported through the exosphere to the hot dayside where they escape. The result is that any H atoms that diffuse through the thermosphere and reach the exobase at any local time, even at very cold locations, are transported to the hot dayside where they escape.

Figure 3b shows that the escape flux varies strongly with local time, but the diurnal average of the calculated escape flux is $2.4\times10^8\,\mathrm{cm^{-2}s^{-1}}$ and this is equal to the limiting flux, reflecting the fact that all H atoms that diffuse to the exobase are subject to Jeans escape from the warm regions of the atmosphere.

## 4. Discussion

The limiting flux proposed here is more accurate than the classical formula but it is also more complicated. For present-day Mars, the classical formula underestimates the limiting flux by roughly a factor of two, dependent on the eddy diffusion and temperature profiles. Given the large number of observations of H on Mars and the high interest in the H escape process, the extra difficulty in calculating the new limiting flux seems worthwhile. Whether the additional accuracy is needed in other applications should be examined on a case-by-case basis.

The role of ballistic flow in the escape rate from Mars cannot be ignored. If the exobase has any region with temperatures high enough to drive rapid escape and, if ballistic transport is efficient, escape is a planet wide phenomenon and the globally integrated escape rate should be equal to the

globally integrated limiting flux. H atoms from cold regions, where escape is negligible, are transported to warm regions, where they easily escape. The arguments presented here are supported by models for the diurnal variation in equatorial regions but the conclusions should apply as well to latitudinal variations. H escape should be diffusion limited everywhere on Mars.

The investigation described here is conceptual, rather than detailed or thorough. The real Mars has numerous complications that we have ignored in order to concentrate on some factors that have received insufficient attention to date. These include but are not limited the chemical conversion of $H_2O$ and $H_2$ to H, non-thermal escape processes, and finite transport times in the thermosphere and exosphere. The calculations of Chaufray et al. (2018) support the assumption that ballistic flow dominates horizontal transport but a wider range of conditions should be studied with a GCM that couples thermospheric calculations with exospheric transport and the processes calculated in the model should be looked at more deeply in light of the concepts presented here. Finally, the models discuss here assume that vertical transport is entirely due to diffusion. We know that advection can deposit $H_2O$ in the upper mesosphere (Stone et al., 2020; Belyaev et al., 2021). At present there are no observations that suggest advection can carry $H_2O$ to the upper thermosphere. The neglect of these processes may complicate but should not negate the conclusions presented here.

The concepts discussed here may have implications for the study of H escape from terrestrial exoplanets and the atmospheres of our own terrestrial planets early in their history. The early Venus atmosphere experienced large solar EUV insolation and should have had higher exospheric temperatures

than present day Venus. In that case escape of H may have been diffusion limited and, given the long length of a day on Venus, thermal escape may only have been efficient on the dayside. Tidally locked terrestrial exoplanets around white dwarf stars may similarly have hot daysides and cold nightsides and escape of H may be an important process, especially for planets with liquid water. If so, the role of ballistic transport must be considered in the escape of these atmospheres.

## Acknowledgements

I thank S. Gupta, E. Cangi and M. Chaffin for helpful conversations.

S. Aoki, A. C. Vandaele, F. Daerden, G. L. Villanueva, G. Liuzzi, I. R. Thomas, J. T. Erwin, L. Trompet, S. Robert, L. Neary, S. Viscardy, R. T. Clancy, M. D. Smith, M. A. Lopez-Valverde, B. Hill, B. Ristic, M. R. Patel, G. Bellucci, and J. J. Lopez-Moreno. Water Vapor Vertical Profiles on Mars in Dust Storms Observed by TGO/NOMAD. *Journal of Geophysical Research (Planets)*, 124(12):3482–3497, Dec. 2019. doi: 10.1029/2019JE006109.

P. Banks and G. Kockarts. *Aeronomy*. Academic Press, San Diego, California, USA, 1973.

D. A. Belyaev, A. A. Fedorova, A. Trokhimovskiy, J. Alday, F. Montmessin, O. I. Korablev, F. Lefèvre, A. S. Patrakeev, K. S. Olsen, and A. V. Shakun. Revealing a High Water Abundance in the Upper Mesosphere of Mars With ACS Onboard TGO. *Geophys. Res. Letts.*, 48(10):e93411, May 2021. doi: 10.1029/2021GL093411.

D. Bhattacharyya, J. T. Clarke, J.-L. Bertaux, J.-Y. Chaufray, and M. Mayyasi. A strong seasonal dependence in the Martian hydrogen exosphere. *Geophys. Res. Letts.*, 42(20):8678–8685, Oct. 2015. doi: 10.1002/2015GL065804.

D. Bhattacharyya, J. Y. Chaufray, M. Mayyasi, J. T. Clarke, S. Stone, R. V. Yelle, W. Pryor, J. L. Bertaux, J. Deighan, S. K. Jain, and N. M. Schneider. Two-dimensional model for the martian exosphere: Applications to hydrogen and deuterium Lyman $\alpha$ observations. *Icarus*, 339:113573, Mar. 2020. doi: 10.1016/j.icarus.2019.113573.

415 D. Bhattacharyya, J. T. Clarke, M. Mayyasi, V. Shematovich, D. Bisikalo,
416 J. Y. Chaufray, E. Thiemann, J. Halekas, C. Schmidt, J. L. Bertaux,
417 M. S. Chaffin, and N. M. Schneider. Evidence of Non-Thermal Hydrogen
418 in the Exosphere of Mars Resulting in Enhanced Water Loss. *Journal of*
419 *Geophysical Research (Planets)*, 128(8):e2023JE007801, Aug. 2023. doi:
420 10.1029/2023JE007801.

421 S. W. Bougher, D. Pawlowski, J. M. Bell, S. Nelli, T. McDunn, J. R. Murphy,
422 M. Chizek, and A. Ridley. Mars Global Ionosphere-Thermosphere Model:
423 Solar cycle, seasonal, and diurnal variations of the Mars upper atmosphere.
424 *Journal of Geophysical Research (Planets)*, 120(2):311–342, Feb. 2015. doi:
425 10.1002/2014JE004715.

426 E. Cangi, M. Chaffin, R. Yelle, B. Gregory, and J. Deighan. Fully Coupled
427 Photochemistry of the Deuterated Ionosphere of Mars and Its Effects on
428 Escape of H and D. *Journal of Geophysical Research (Planets)*, 128(7):
429 e2022JE007713, July 2023. doi: 10.1029/2022JE007713.

430 M. S. Chaffin, J.-Y. Chaufray, I. Stewart, F. Montmessin, N. M. Schnei-
431 der, and J.-L. Bertaux. Unexpected variability of Martian hydro-
432 gen escape. *Geophys. Res. Letts.*, 41(2):314–320, Jan. 2014. doi:
433 10.1002/2013GL058578.

434 M. S. Chaffin, J. Deighan, N. M. Schneider, and A. I. F. Stewart. El-
435 evated atmospheric escape of atomic hydrogen from Mars induced by
436 high-altitude water. *Nature Geoscience*, 10(3):174–178, Jan. 2017. doi:
437 10.1038/ngeo2887.

M. S. Chaffin, D. M. Kass, S. Aoki, A. A. Fedorova, J. Deighan, K. Connour, N. G. Heavens, A. Kleinböhl, S. K. Jain, J. Y. Chaufray, M. Mayyasi, J. T. Clarke, A. I. F. Stewart, J. S. Evans, M. H. Stevens, W. E. McClintock, M. M. J. Crismani, G. M. Holsclaw, F. Lefevre, D. Y. Lo, F. Montmessin, N. M. Schneider, B. Jakosky, G. Villanueva, G. Liuzzi, F. Daerden, I. R. Thomas, J. J. Lopez-Moreno, M. R. Patel, G. Bellucci, B. Ristic, J. T. Erwin, A. C. Vandaele, A. Trokhimovskiy, and O. I. Korablev. Martian water loss to space enhanced by regional dust storms. *Nature Astronomy*, 5:1036–1042, Oct. 2021. doi: 10.1038/s41550-021-01425-w.

J. Chamberlain and D. Hunten. *Theory of Planetary Atmospheres: An Introduction to their Physics and Chemistry*. Academic Press, San Diego, California, USA, 1986.

J. Y. Chaufray, F. Gonzalez-Galindo, F. Forget, M. A. Lopez-Valverde, F. Leblanc, R. Modolo, and S. Hess. Variability of the hydrogen in the martian upper atmosphere as simulated by a 3D atmosphere-exosphere coupling. *Icarus*, 245:282–294, Jan. 2015. doi: 10.1016/j.icarus.2014.08.038.

J. Y. Chaufray, R. V. Yelle, F. Gonzalez-Galindo, F. Forget, M. Lopez-Valverde, F. Leblanc, and R. Modolo. Effect of the Lateral Exospheric Transport on the Horizontal Hydrogen Distribution Near the Exobase of Mars. *Journal of Geophysical Research (Space Physics)*, 123(3):2441–2454, Mar. 2018. doi: 10.1002/2017JA025163.

J. T. Clarke, J. L. Bertaux, J. Y. Chaufray, G. R. Gladstone, E. Quemerais, J. K. Wilson, and D. Bhattacharyya. A rapid decrease of the hydrogen

corona of Mars. *Geophys. Res. Letts.*, 41(22):8013–8020, Nov. 2014. doi: 10.1002/2014GL061803.

F. D. Colegrove, W. B. Hanson, and F. S. Johnson. Eddy Diffusion and Oxygen Transport in the Lower Thermosphere. *Journal of Geophysical Research*, 70(19):4931–4941, Oct. 1965. doi: 10.1029/JZ070i019p04931.

J. Cui, R. V. Yelle, and K. Volk. Distribution and escape of molecular hydrogen in Titan's thermosphere and exosphere. *Journal of Geophysical Research (Planets)*, 113(E10):E10004, Oct. 2008. doi: 10.1029/2007JE003032.

M. K. Elrod, S. Bougher, J. Bell, P. R. Mahaffy, M. Benna, S. Stone, R. Yelle, and B. Jakosky. He bulge revealed: He and $CO_2$ diurnal and seasonal variations in the upper atmosphere of Mars as detected by MAVEN NGIMS. *Journal of Geophysical Research (Space Physics)*, 122(2):2564–2573, Feb. 2017. doi: 10.1002/2016JA023482.

A. Fedorova, J.-L. Bertaux, D. Betsis, F. Montmessin, O. Korablev, L. Maltagliati, and J. Clarke. Water vapor in the middle atmosphere of Mars during the 2007 global dust storm. *Icarus*, 300:440–457, Jan. 2018. doi: 10.1016/j.icarus.2017.09.025.

A. A. Fedorova, F. Montmessin, O. Korablev, M. Luginin, A. Trokhimovskiy, D. A. Belyaev, N. I. Ignatiev, F. Lefèvre, J. Alday, P. G. J. Irwin, K. S. Olsen, J.-L. Bertaux, E. Millour, A. Määttänen, A. Shakun, A. V. Grigoriev, A. Patrakeev, S. Korsa, N. Kokonkov, L. Baggio, F. Forget, and C. F. Wilson. Stormy water on Mars: The distribution and saturation of

484 atmospheric water during the dusty season. *Science*, 367(6475):297–300,
485 Jan. 2020. doi: 10.1126/science.aay9522.

486 J. L. Fox. On the escape of oxygen and hydrogen from Mars. *Geophys. Res.*
487 *Letts.*, 20(17):1747–1750, Sept. 1993. doi: 10.1029/93GL01118.

488 J. C. Gérard, S. W. Bougher, M. A. López-Valverde, M. Pätzold, P. Drossart,
489 and G. Piccioni. Aeronomy of the Venus Upper Atmosphere. *Space Science*
490 *Reviews*, 212(3-4):1617–1683, Nov. 2017. doi: 10.1007/s11214-017-0422-0.

491 N. Gupta, N. V. Rao, S. Bougher, and M. K. Elrod. Latitudinal and Sea-
492 sonal Asymmetries of the Helium Bulge in the Martian Upper Atmosphere.
493 *Journal of Geophysical Research (Planets)*, 126(10):e06976, Oct. 2021. doi:
494 10.1029/2021JE006976.

495 J. S. Halekas. Seasonal variability of the hydrogen exosphere of Mars. *Jour-*
496 *nal of Geophysical Research (Planets)*, 122(5):901–911, May 2017. doi:
497 10.1002/2017JE005306.

498 N. G. Heavens, A. Kleinböhl, M. S. Chaffin, J. S. Halekas, D. M. Kass, P. O.
499 Hayne, D. J. McCleese, S. Piqueux, J. H. Shirley, and J. T. Schofield.
500 Hydrogen escape from Mars enhanced by deep convection in dust storms.
501 *Nature Astronomy*, 2:126–132, Feb. 2018. doi: 10.1038/s41550-017-0353-4.

502 J. Hodges, R. R. and F. S. Johnson. Lateral transport in planetary exo-
503 spheres. *Journal of Geophysical Research*, 73(23):7307, Jan. 1968. doi:
504 10.1029/JA073i023p07307.

505 D. M. Hunten. The Escape of Light Gases from Planetary Atmospheres.

*Journal of Atmospheric Sciences*, 30(8):1481–1494, Nov. 1973. doi: 10.1175/1520-0469(1973)030¡1481:TEOLGF¿2.0.CO;2.

B. M. Jakosky. Atmospheric Loss to Space and the History of Water on Mars. *Annual Review of Earth and Planetary Sciences*, 49, May 2021. doi: 10.1146/annurev-earth-062420-052845.

V. A. Krasnopolsky. Solar Cycle Variations of the Hydrogen Escape Rate and the CO Mixing Ratio on Mars. *Icarus*, 101(1):33–41, Jan. 1993. doi: 10.1006/icar.1993.1003.

J. Park, J. S. Evans, R. W. Eastes, J. D. Lumpe, J. van den Ijssel, C. R. Englert, and M. H. Stevens. Exospheric Temperature Measured by NASA-GOLD Under Low Solar Activity: Comparison With Other Data Sets. *Journal of Geophysical Research (Space Physics)*, 127(3):e30041, Mar. 2022. doi: 10.1029/2021JA030041.

K. J. Roeten, S. W. Bougher, M. Benna, P. R. Mahaffy, Y. Lee, D. Pawlowski, F. González-Galindo, and M. Á. López-Valverde. MAVEN/NGIMS Thermospheric Neutral Wind Observations: Interpretation Using the M-GITM General Circulation Model. *Journal of Geophysical Research (Planets)*, 124(12):3283–3303, Dec. 2019. doi: 10.1029/2019JE005957.

S. W. Stone, R. V. Yelle, M. Benna, M. K. Elrod, and P. R. Mahaffy. Thermal Structure of the Martian Upper Atmosphere From MAVEN NGIMS. *Journal of Geophysical Research (Planets)*, 123(11):2842–2867, Nov. 2018. doi: 10.1029/2018JE005559.

S. W. Stone, R. V. Yelle, M. Benna, D. Y. Lo, M. K. Elrod, and P. R. Mahaffy. Hydrogen escape from Mars is driven by seasonal and dust storm transport of water. *Science*, 370(6518):824–831, Nov. 2020. doi: 10.1126/science.aba5229.

S. W. Stone, R. V. Yelle, M. Benna, M. K. Elrod, and P. R. Mahaffy. Neutral Composition and Horizontal Variations of the Martian Upper Atmosphere From MAVEN NGIMS. *Journal of Geophysical Research (Planets)*, 127 (6):e07085, June 2022. doi: 10.1029/2021JE007085.

K. Zahnle, R. M. Haberle, D. C. Catling, and J. F. Kasting. Photochemical instability of the ancient Martian atmosphere. *Journal of Geophysical Research (Planets)*, 113(E11):E11004, Nov. 2008. doi: 10.1029/2008JE003160.

## Appendix A. Appendix

The vertical diffusion equation is

$$\Phi_i = -D_i \left[ \frac{dN_i}{dr} + N_i \left( \frac{1}{H_i} + \frac{1}{T}\frac{dT}{dr} \right) \right] - K \left[ \frac{dN_i}{dr} + N_i \left( \frac{1}{H_a} + \frac{1}{T}\frac{dT}{dr} \right) \right] \tag{A.1}$$

where variables are defined in the main text. The scale height is related to the temperature and molecular mass through

$$H_i = \frac{kT}{m_i g}\,, \tag{A.2}$$

The quantity $H_a$ is pressure scale height for the atmosphere, defined by

$$H_a = \frac{kT}{m_a g}\,, \tag{A.3}$$

where $m_a$ is the mean molecular weight of the atmosphere (averaged over all constituents). Each individual species satisfies the ideal gas law

$$P_i = N_i kT \tag{A.4}$$

and it follows that the bulk atmosphere does as well

$$P_a = N_a kT \tag{A.5}$$

It is frequently more convenient to use mole fractions $X_i$ in place of density in the diffusion equation. The mole fraction is related to the density through

$$N_i = X_i N_a \tag{A.6}$$

and it follows that

$$\frac{dN_i}{dr} = N_a \frac{dX_i}{dr} + X_i \frac{dN_a}{dr} \tag{A.7}$$

Using the ideal gas law we have

$$\frac{dN_a}{dr} = \frac{1}{kT}\frac{dP_a}{dr} - \frac{P_a}{kT^2}\frac{dT}{dr} \tag{A.8}$$

Substituting equations A.6, A.7, and A.8 into equation A.1 gives

$$\frac{\Phi_i}{N_a} = -\left(D_i + K\right)\frac{dX_i}{dr} + D\frac{(m_a - m_i)g}{kT}X_i, \tag{A.9}$$

which is actually quite a bit simpler than equation 1. Notice that the temperature gradient no longer appears in the equation.

Next, the vertical variable is changed from altitude to the log of atmospheric pressure:

$$\zeta = -\ln\left(P_a/P_\circ\right) \tag{A.10}$$

where $P_\circ$ is an arbitrary reference pressure. We have

$$\frac{d}{dr} = \frac{dy}{dr}\frac{d}{d\zeta} = \frac{m_a g}{kT}\frac{d}{d\zeta} \tag{A.11}$$

and

$$\frac{dX_i}{d\zeta} + \frac{D_i(m_i/m_a - 1)}{D_i + K}X_i + \frac{r^2\Phi_i kT}{GMm_a N_a(D_i + K)} = 0. \tag{A.12}$$

We now restrict our analysis to situations where the diffusion dominates over chemistry. The 1D continuity equation is

$$\frac{\partial N_i}{\partial t} = P_i - L_i - \frac{1}{r^2}\frac{\partial}{\partial r}r^2\Phi_i \tag{A.13}$$

In steady-state and assume that chemistry can be neglected we have

$$r^2\Phi_i = r_\circ^2\Phi_i^\circ = \text{constant} \tag{A.14}$$

where $r_\circ$ is an arbitrary reference level and $\Phi_i^\circ$ is the flux at that level. Substituting into equation A.12 gives

$$\frac{dX_i}{d\zeta} + \frac{D_i(m_i/m_a - 1)}{D_i + K}X_i + \frac{r_\circ^2\Phi_i^\circ kT}{GMm_a N_a(D_i + K)} = 0\,, \tag{A.15}$$

which is equation 2 in the main text.

If $\Phi_i^\circ = 0$ then equation A.15 can be integrated to give

$$\tilde{X}_i(\zeta) = C \exp\left\{ \left( \left(1 - \frac{m_i}{m_a}\right) \int_0^\zeta \frac{D_i(\zeta')}{D_i(\zeta') + K(\zeta')} \, d\zeta' \right) \right\}, \tag{A.16}$$

which is equation 9 in the main text. The solution to equation A.15 for $\Phi_i^\circ \neq 0$ can be found by defining

$$X_i(\zeta) = W(\zeta)\tilde{X}_i(\zeta) \tag{A.17}$$

from which is follows that

$$\frac{dX_i}{d\zeta} = \tilde{X}_i \frac{dW}{d\zeta} + W \frac{d\tilde{X}_i}{d\zeta} \,. \tag{A.18}$$

Substitution into equation A.15 gives

$$\tilde{X}_i \frac{dW}{d\zeta} + W \frac{d\tilde{X}_i}{d\zeta} + \frac{D_i(m_i/m_a - 1)}{D_i + K} \tilde{X}_i W + \frac{r_\circ^2 \Phi_i^\circ kT}{GMm_a N_a (D_i + K)} = 0 \,. \tag{A.19}$$

or

$$\tilde{X}_i \frac{dW}{d\zeta} + W \left( \frac{d\tilde{X}_i}{d\zeta} + \frac{D_i(m_i/m_a - 1)}{D_i + K} \tilde{X}_i \right) + \frac{r_\circ^2 \Phi_i^\circ kT}{GMm_a N_a (D_i + K)} = 0 \,. \tag{A.20}$$

or

$$\tilde{X}_i \frac{dW}{d\zeta} + W \left( 0 \right) + \frac{r_\circ^2 \Phi_i^\circ kT}{GMm_a N_a (D_i + K)} = 0 \,. \tag{A.21}$$

and

$$\tilde{X}_i \frac{dW}{d\zeta} + \frac{r_\circ^2 \Phi_i^\circ kT}{GMm_a N_a (D_i + K)} = 0 \,. \tag{A.22}$$

and

$$W(\zeta) = 1 - \int_0^\zeta \frac{1}{\tilde{X}_i(\zeta')} \frac{r_\circ^2 \Phi_i^\circ kT(\zeta')}{GMm_a(\zeta') N_a(\zeta') (D_i(\zeta') + K(\zeta'))} \, d\zeta' \,, \tag{A.23}$$

and

$$X_i(\zeta) = \tilde{X}_i(\zeta) - \int_0^\zeta \frac{\tilde{X}_i(\zeta)}{\tilde{X}_i(\zeta')} \frac{r_\circ^2 \Phi_i^\circ kT(\zeta')}{GMm_a(\zeta')N_a(\zeta')(D_i(\zeta') + K(\zeta'))}\, d\zeta' \,, \quad \text{(A.24)}$$

Equation A.24 can be made a little nicer by defining

$$g(\zeta) \equiv \int_0^\zeta \frac{kT(\zeta')r_\circ^2\, d\zeta'}{\tilde{X}_i(\zeta')\big(D_i(\zeta') + K(\zeta')\big)N_a(\zeta')GMm_a} \,, \quad \text{(A.25)}$$

then

$$X_i(\zeta) = \tilde{X}_i(\zeta)\Big(1 - g(\zeta)\Phi_i^\circ\Big) \,. \quad \text{(A.26)}$$

Equations A.25 and A.26 are equations 10 and 8 in the main text.

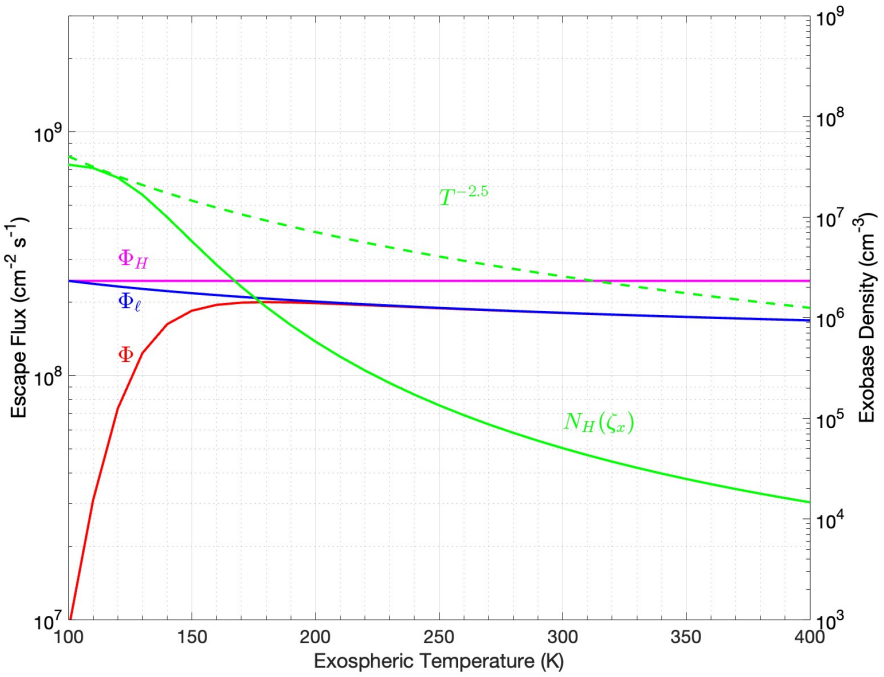


Figure A.1: Escape fluxes as a function of exospheric temperature from our 1D model for the Mars atmosphere. The red curve shows the escape flux calculated with our 1D model, the blue curve, the limiting flux proposed here, and the magenta curve, the classical limiting flux. The solid green curve shows the H density at the exobase calculated with our 1D model. The dashed green curve shows the variation of density with exobase temperature implied by the Hodges et al. relationship. Fluxes are referred to the surface. Temperatures and densities are at the exobase.

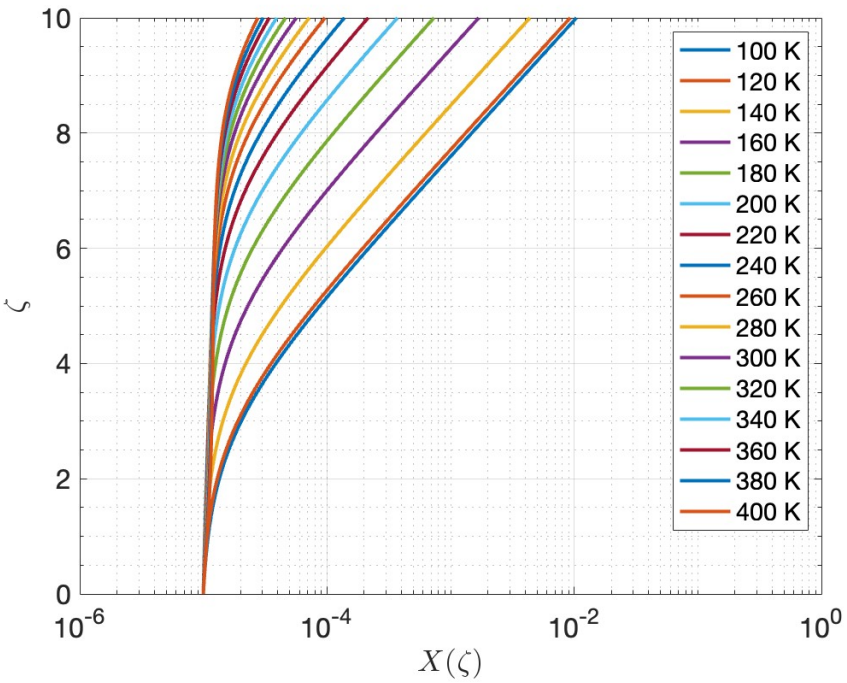


Figure A.2: The variation of H mole fraction with $\zeta$ for various values of the exospheric temperature.

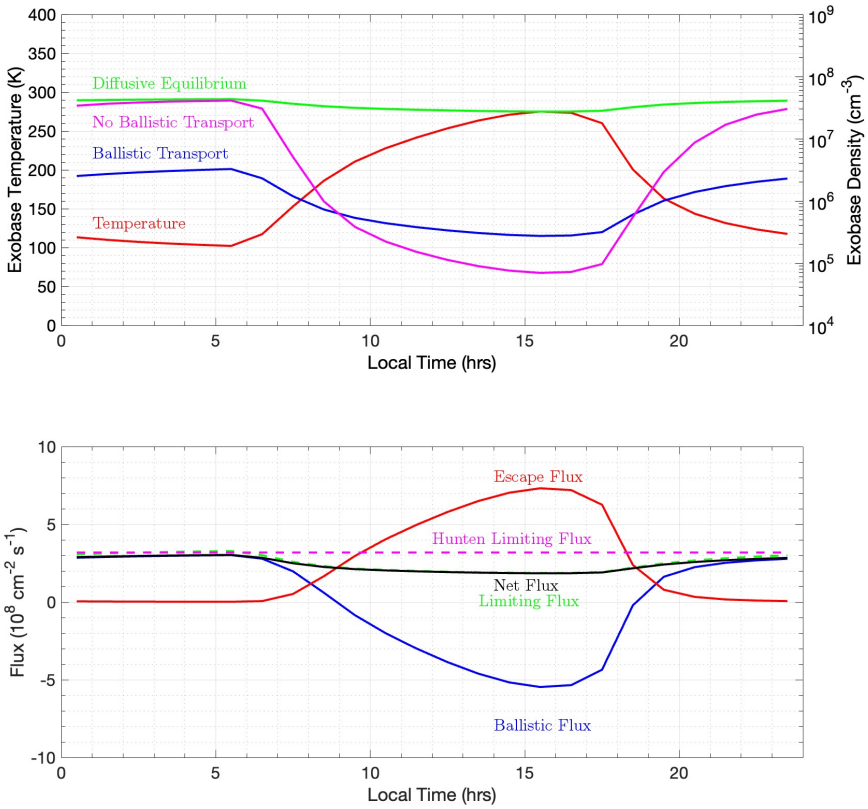


Figure A.3: a) The red curve shows the exobase temperature as a function of local time from Stone et al. (2018). The magenta curve shows the calculated density without ballistic fluxes, using the Jeans flux as the boundary condition. The blue curve shows the exobase density calculated with ballistic fluxes adjusted so that the density follows the $T^{-2.5}$ variation. The green curve shows the diffusive equilibrium solution. b) The red curve shows the escape flux calculated with our 2D model. The blue curve is the net ballistic flux in that model and the black curve is the sum of escape and ballistic fluxes.

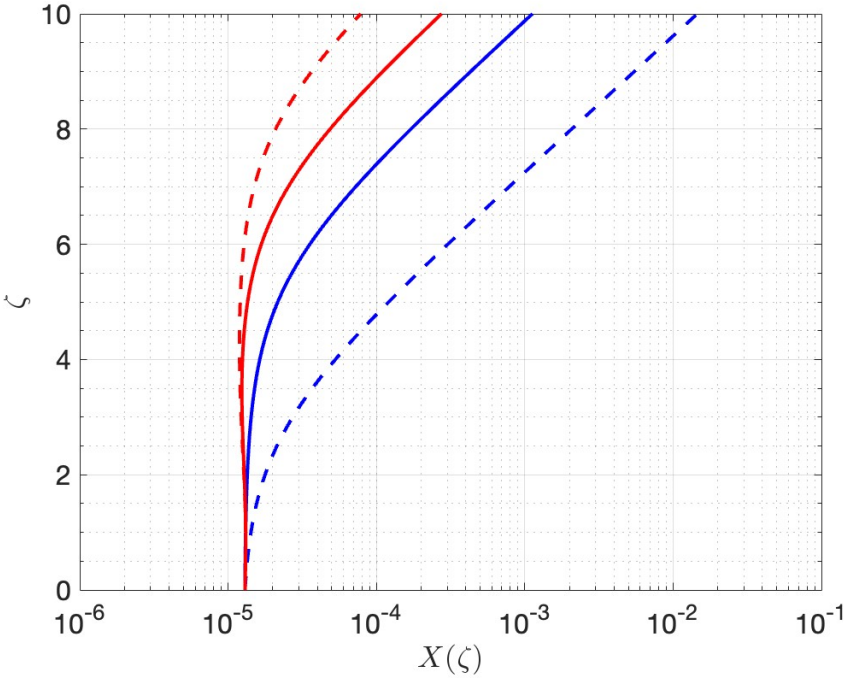


Figure A.4: The H mole fraction versus negative log pressure ($\zeta$) at local times of 3:30 AM (blue) and 3:30 PM (red). The dashed lines show the result of calculations assuming only the Jeans boundary condition, the solid line the result of calculations including ballistic fluxes adjusted to match the Hodges and Johnson (1968) relationship. Upward ballistic flow at 3:30 AM results in a decrease of the H mole fraction at high altitude while downward ballistic flow at 3:30 PM results in an increase of the H mole fraction at high altitude.

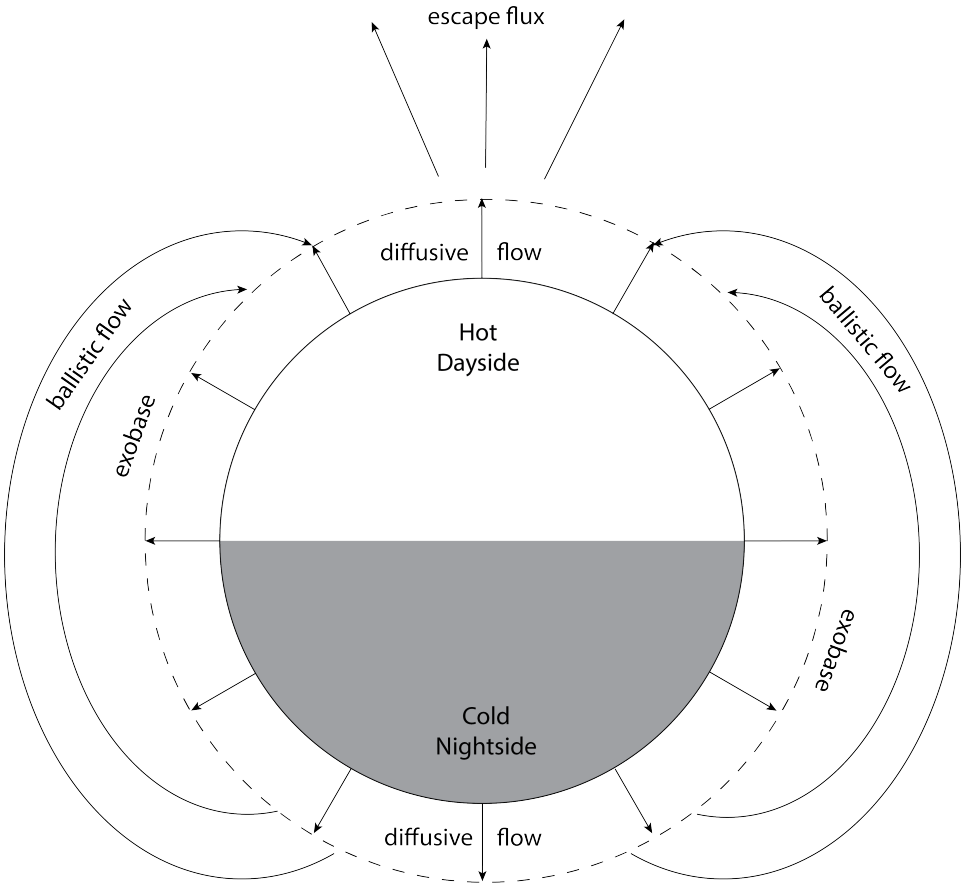


Figure A.5: A cartoon showing the H fluxes associated with escape on Mars. Diffusive flow is upwards everywhere in the thermosphere. The H atoms that reach the exobase on the nightside are transported to the dayside where they are rapidly lost by Jeans escape.